IEEE Access
Multidisciplinary | Rapid Review | Open Access Journal

Received May 11, 2018, accepted June 8, 2018, date of publication June 18, 2018, date of current version July 6, 2018.

Digital Object Identifier 10.1109/ACCESS.2018.2848476

A Dual-Wideband and High Gain Magneto-Electric Dipole Antenna and Its 3D MIMO System With Metasurface for 5G/WiMAX/WLAN/X-Band Applications

BOTAO FENG[1], (Member, IEEE), JIEXIN LAI[1], QINGSHENG ZENG[2], (Senior Member, IEEE), AND KWOK L. CHUNG[3], (Senior Member, IEEE)

[1]College of Electronic Science and Technology, Shenzhen University, Shenzhen 518060, China
[2]College of Aeronautics, Nanjing University of Aeronautics and Astronautics, Nanjing 210016, China
[3]School of Communications and Electronic Engineering, Qingdao University of Technology, Qingdao 266033, China

Corresponding author: Qingsheng Zeng (qingshengzeng@nuaa.edu.cn)

This work was supported in part by the Natural Science Foundation of Guangdong Province, China, under Grant 2016A030310056, in part by the Key Project of Department of Education of Guangdong Province under Grant 2015KTSCX123, in part by the Fundamental Research Foundation of Shenzhen under Grant JCYJ20160308100236349, in part by the Natural Science Foundation of SZU under Grant 2016021, and in part by the NTUT-SZU Joint Research Program under Grant 2018002.

ABSTRACT A substrate integrated magneto-electric (ME) dipole antenna with metasurface is proposed for the 5G/WiMAX/WLAN/X-band MIMO applications. In order to provide a low profile, the radiated electric dipoles integrated with shorted wall are used in the multi-layer substrates at different heights. Owing to the coordination of the metasurface and the ME dipole, dual wideband and high gain have been obtained. As a result of the 3-D hexagonal structure, good envelope correlation coefficient and mean effective gain performance can be achieved by the MIMO antenna system. The antenna element can provide an impedance bandwidth of 66.7% (3.1–6.2 GHz) with a stable gain of 7.6 ± 1.5 dBi and an impedance bandwidth of 20.3% (7.1–8.7 GHz) with a gain of 7.4 ± 1.8 dBi for the lower and upper bands, respectively. The overall size of the element is $60 \times 60 \times 7.92$ mm^3. Hence, it is well-suited for the future 5G/WiMAX/WLAN/X-band MIMO communications.

INDEX TERMS Metasurface antenna, magneto-electric antenna, MIMO antenna, low profile, high gain.

I. INTRODUCTION

With the explosive growing need of high-speed data transmission and the coexistence of many different kinds of wireless networks such as the WiMAX/WLAN/X-Band systems, multi-frequency and wideband mobile communication system is in urgent need. The Sub-6GHz frequency bands (3.4-3.6 GHz and 4.8-5 GHz) have been allocated as the fifth generation mobile communication in China since November 2017 [1]. Hence, many literatures about 5G wideband antennas have been reported in the aforementioned bands [2]–[6]. Besides, due to the outstanding advantages such as enhancing channel capacity, improving the performances of transmitting and receiving signals, arranging massive antennas into a limited space and so on, the MIMO technology has been widely studied for 5G application. Recently, several literatures on 5G MIMO antennas for smart phone and base-station have been proposed by Profs. Ban *et al.* [2], Li *et al.* [3], Chen and Luk [7], Liang *et al.* [8], and Zhu *et al.* [9]. In order to improve the system capacity, by introducing four quad-antenna linear arrays which are disposed along two edges of the system circuit board of the smartphone, a 16-antenna array operated in the 3.5 GHz C-band is presented in [4]. To provide the three-dimensional (3D) coverage, a wideband ranging from 1.77 GHz to 2.62 GHz can be achieved by arranging the five ME dipole antenna elements on a cubic surface in [7]. However, few literatures on the MIMO antenna for 5G/WiMAX/WLAN/X-Band communication have been reported owing to its design difficulty in such a wideband [10]–[12].

Because of its splendid characteristics, such as low cross-polarization, high gain as well as complementary

E- and H-plane unidirectional radiation patterns, etc, the magneto-electric (ME) dipole antenna proposed by Profs. Luk and Wong, has been extensively studied in the past few years [7], [13]–[15]. However, the structures of conventional ME dipole antennas are somewhat bulky and still cannot be used for 5G frequency band. On the other hand, the miniaturized mobile electronic devices have been integrated in a high density to realize multiple functions owing to the increasing demand for smart communication systems [16]–[18]. Hence, substrate-integrated technology is one of the most popular miniaturized technologies and has been widely used in antenna design. By employing a tapered H-shaped ground co-operated with substrate-integrated technology, the thickness of the proposed ME dipole antenna can be highly reduced from $0.25\lambda_0$ to $0.11\lambda_0$ in [16] (where λ_0 is the free-space wavelength at the initial frequency). In [18], an improved bow-tie patch based on multi-layer substrate-integrated technology together with the via holes structure is adopted to obtain an impedance bandwidth of 110% with SWR$\leq$2 from 3.1-10.66 GHz and a stable gain of 8.4$\pm$2.5 dBi. Owing to the above-mentioned technology, some advantages including low cost, easy fabrication and good reliability can be easily achieved. However, so far, the multi-layer integrated technology is rarely applied in MIMO ME antenna design due to the complicated structure and challenging performance.

More recently, due to its outstanding electromagnetic characteristics such as miniaturization, frequency reconfiguration, pattern reconfiguration, improving gain and so on, metamaterials have attracted much attention in many fields [19]–[23]. A lot of achievements on the metamaterial antenna have been made by Profs. Chung and Zhu, etc. By adopting the window-shaped metasurface array patches which are arranged in an air-gap structure, signals can easily be converted between linearly polarization (LP) and circularly polarization in a wide frequency band [19]. Then, by introducing the rectangular-ring lens printed on both sides of a circular substrate, the gain can be significantly improved by 5 dB [20]. In order to achieve the miniaturization, the split-ring resonator (SRR) metamaterial loadings are placed in the center of the ME dipole antenna [22]. As a result, the antenna size can be reduced by 48% and a wide bandwidth of 44% with a gain of about 8.5 dBi can be acquired. To sum up, metamaterial structure helps to significantly improve both the functionality and the performance of the antenna.

In this paper, in order to provide the high gain and low profile performances in the desired wideband, a substrate integrated ME dipole antenna with metasurface is proposed for the 5G/WiMAX/WLAN/X-Band MIMO applications. Firstly, to provide the low profile characteristic, the radiated electric dipoles and the shorted wall are integrated in the multi-layer substrates. In addition, owing to the coordination of the metasurface and the ME dipole, the dual wideband and high gain features can be easily achieved. Finally, as a result of the 3D hexagonal structure whose design is based on the beam steering concept, the good ECC and MEG performance can be obtained by the MIMO antenna system. Also, a 360° omnidirectional coverage in the operating frequency bands can be acquired. With the above-mentioned features, it is a powerful competitor for the 5G/WiMAX/WLAN/X-Band MIMO applications.

II. ANTENNA GEOMETRY AND WORKING MECHANISM

A. ANTENNA ELEMENT

As shown in Fig. 1, the proposed antenna is printed on the three-layer Rogers 5880 substrate with a dielectric constant of $\xi_r = 2.2$ and a loss tangent of $\delta = 9\times10^{-4}$. From top to bottom, their thicknesses are 1.52 mm, 3.75 mm and 3.75 mm, respectively. The total size of the antenna element is $60\times60\times7.92$ mm^3. Basically, the proposed antenna element consists of an arc-shaped electric dipole radiated patch etched with zigzagged slot, a pair of via hole shorted walls, an η-shaped feeding structure, a metasurface patch and a ground plane. The arc-shaped electric dipole radiated patch with zigzagged slot collaborates with the I-shaped metasurface to provide dual wideband characteristics. As shown in Fig. 1(b), the pair of via-hole shorted walls and the ground between them form a basic magnetic dipole. The feeding structure which comprises a transmission line and a fork-shaped coupling strip is introduced to excite the ME dipole. The fork-shaped feeding structure can easily provide flexible impedance matching and energy coupling. As for a typical ME dipole antenna, its complementary radiation pattern is shown in Fig. 2 [24]. In the E-plane, the radiation pattern of an electric dipole exhibits an ''8'' shape while the one of magnetic dipole displays an ''O'' shape. And in the H-plane, the situation is vice versa. When the two sources with equal amplitude work together, a cardiac shape radiation pattern can be realized in alternation in both the E-plane and the H-plane. In other words, the complementary unidirectional radiation pattern can be generated. The metasurface patch is made up of 32 pieces of I-shaped patches, which are used to improve the antenna gain and reduce the height of the antenna. However, the metasurface has a slight influence on the bandwidth.

B. MIMO ANTENNA SYSTEM

By using the stable H-plane with an angle of 60° of the proposed element, six-element MIMO antenna system which can provide a 360° full coverage in H-plane is presented, as shown in Fig. 1(d). In order to provide an excellent isolation in the limited storage space, the six elements are arranged on the surface of an orthohexagon at regular intervals. As a result, the mutual coupling between the elements can be effectively eliminated and hence the performance of the envelope correlation coefficient (ECC) constant which is a key parameter of a MIMO antenna system is excellent. Owing to the inherent nature of the ME dipole and the special orthohexagon-shaped design, the MIMO antenna system can afford the stable high gain, a 360° full coverage in H-plane

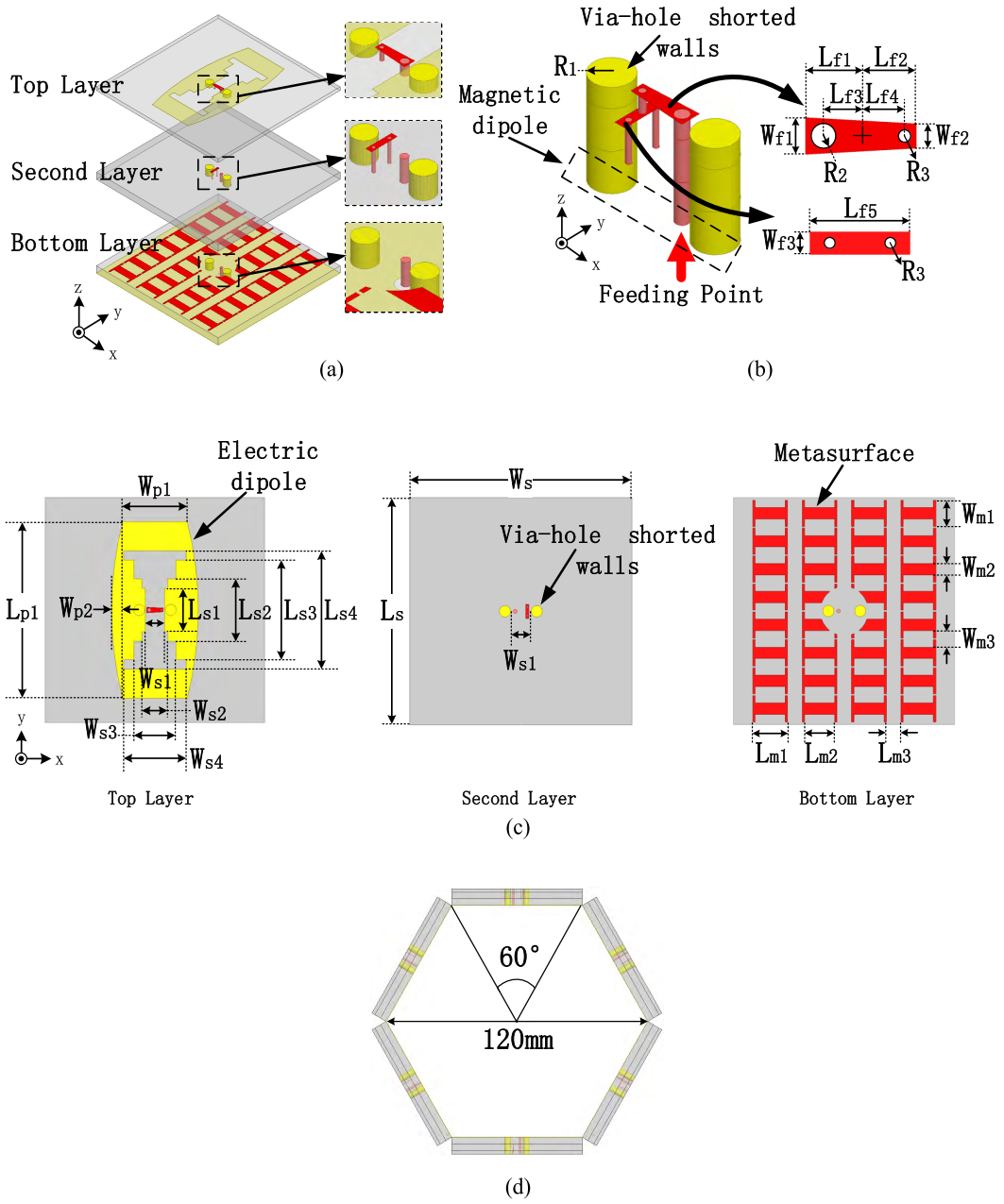

FIGURE 1. Geometry of the proposed antenna and its MIMO system. (a) The 3D perspective. (b) The feeding structure. (c) Top view of each layer. (d) side view of the MIMO system.

with unidirectional radiated pattern, and a low ECC parameter in a compact size.

Table 1 lists the detailed dimensions of the antenna and its MIMO system.

III. PARAMETRIC STUDY

In order to investigate how the the dimensions and different structures affect the antenna performances such as wide impedance bandwidths, stable gains, better radiation patterns and diversity performances, some key parameters are chosen to study by Ansoft High Frequency Structure Simulation (HFSS) [25].

A. EFFECT OF THE ELECTRIC DIPOLES WITH THE ZIGZAGGED SLOTS

1) THE WORK MECHANISM OF ELECTRIC DIPOLES WITH THE ZIGZAGGED SLOTS

The current distributions on the electric dipole with the zigzagged slot at 3.4 GHz, 6.6 GHz and 7.8 GHz over a period are shown in Fig. 3, respectively and they help to reveal the working mechanism. Figs. 3(a1)-3(a3) show the current distributions with the proposed metasurface (MS) while the ones without a MS are shown in Figs. 3(b1)-3(b3). Fig. 3(a1) shows that at t = 0, the currents on the outer edges of the dipole which flow upward enhance while they

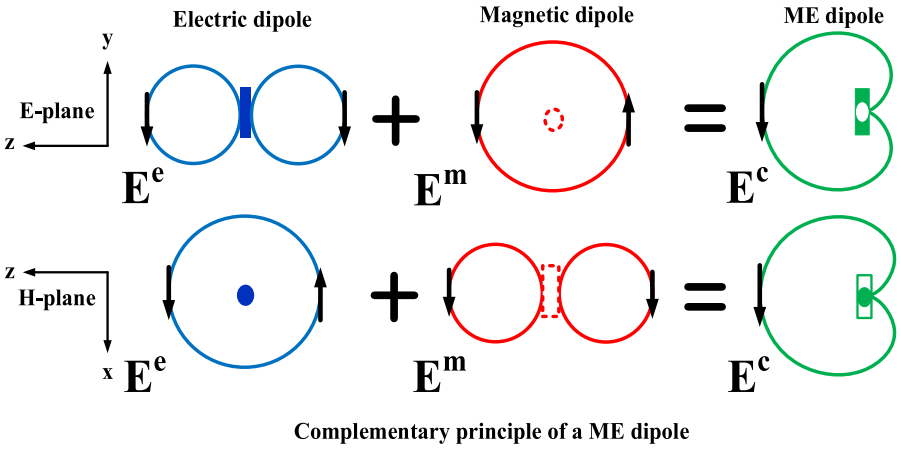

FIGURE 2. Complementary radiation principle of a ME dipole.

TABLE 1. Dimensions for the proposed antenna.

Parameters	L_s	W_s	L_p	W_{p1}	W_{p2}	L_{s1}	L_{s2}
Values/mm	60	60	47.23	17.62	3.04	11.55	16.55
Parameters	L_{s3}	L_{s4}	W_{s1}	W_{s2}	W_{s3}	W_{s4}	L_{f1}
Values/mm	26.55	31.75	5.2	7.06	11.5	17.05	2.16
Parameters	L_{f2}	L_{f3}	L_{f4}	L_{f5}	W_{f1}	W_{f2}	W_{f3}
Values/mm	2.1	1.55	1.75	3.74	1.47	1	0.8
Parameters	W_{f4}	L_{m1}	L_{m2}	L_{m3}	W_{m1}	W_{m2}	W_{m3}
Values/mm	2.26	9.4	8.16	3.95	6.91	3	4.37
Parameters	H_1	H_2	H_3	R_1	R_2	R_3	R_s
Values/mm	1.57	3.175	3.175	1.5	0.5	0.25	6.5

become weaker and turn to be downward at t = T/4. Then at t = T/2, their direction keeps downward and the intensity increases again. Finally, at t = 3T/4, the current intensity decreases and the current direction turns to be upward. As shown in Fig. 3(a3), at 7.8 GHz, the changing situation of current intensity is the same as the one at 3.4 GHz while the directions of the current are in the opposite to the ones at both t = 0 and t = T/2. In other words, the radiated dipoles display the complementary linearly polarized radiation characteristic. However, at the band-notch frequency of 6.6 GHz, the situation is different from those at the lower and upper frequency bands. As shown in Fig. 3(a2), at t = 0, both the currents on the edges and in the center flow downward and the current intensity in the center reaches the maximum. Then, at t = T/4, the direction of the currents on the edges keeps downward while the one in the center turns to be upward. Hence they cancel out each other and the resonant frequency vanishes. In addition, the current intensity becomes minimum. At t = T/2, both the currents on the edges and in the center flow upward and the current intensity in the center gets maximum again. Finally, at t = 3T/4, the direction of the currents on the edges keeps upward while the one in the center turns to be downward. Hence, they offset each other and the resonant frequency vanishes again. Similar to it at t = T/4, the current intensity turns to be minimum once more. Without a MS, the current distributions at 3.4 GHz and 7.8 GHz are nearly the same as the corresponding ones with a MS. However, the situation without a MS is different from that with a MS at the 6.6 GHz. At t = 0, the currents are mainly in the downward direction and their intensity becomes maximum. Then, at t = T/4, the current direction turns to be upward and the intensity gets minimum. At t = T/2, the current direction keeps constant and the intensity becomes maximum again. Finally, at t = 3T/4, the current direction turns to be in the opposite and the intensity gets minimum once again. That is to say, without a MS, the electric dipoles exhibit the complementary linearly polarized radiation feature in a continuous wide frequency band. On the contrary, with a MS, the complementary linearly polarized radiation feature can only be achieved in the lower and upper frequency bands, respectively.

Fig. 4 shows that at the lower frequency band, with the proposed slot, there is the slightest fluctuations in the SWR and hence the widest bandwidth can be obtained. Correspondingly, the gain is the most stable and the highest at the lower frequency band. On the other hand, at the upper frequency band, with both of the proposed slot and the zigzagged slot, much wider bandwidth and the more stable gain can be achieved, while the condition is opposite by using the arc-shaped slot. To obtain the stable gain and the widest bandwidth in the desired band, the proposed slot is chosen. In conclusion, this is caused by the increased effective electric length and flexible impedance matching. In addition, the arc-height (W_{p2}) is a key parameter of the dipole patch to the bandwidth and gain, as shown in Fig. 5. As the arc-height (W_{p2}) increases, the whole curve moves towards the lower frequency band. Similarly, too small or too large a W_{p2} (eg. W_{p2} = 1.04 mm or W_{p2} = 4.04 mm) will cause an

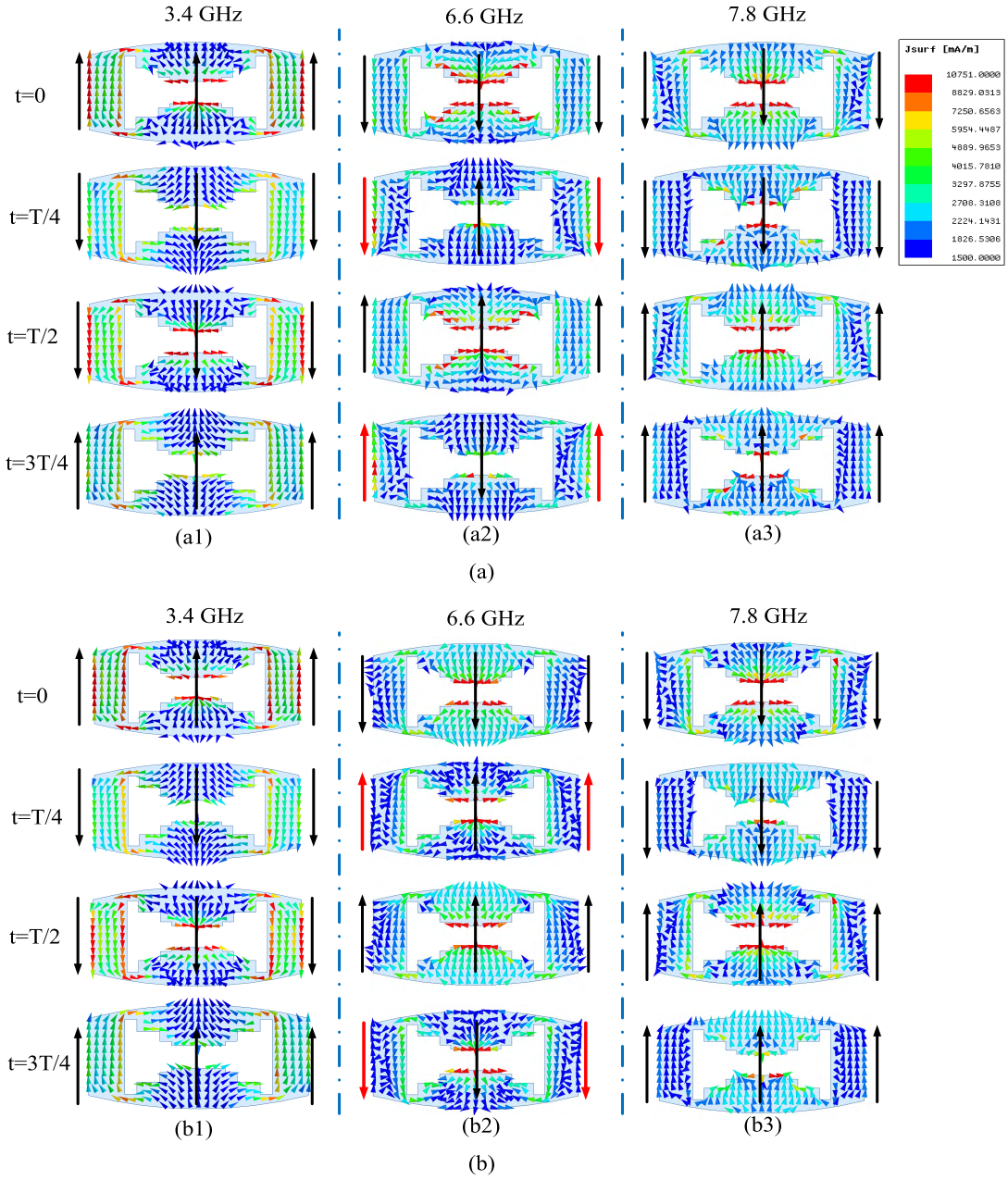

FIGURE 3. Current distributions on the electric dipoles. (a) With the MS. (b) Without the MS.

unstable SWR. Correspondingly, there are significant fluctuations in gain and hence the impedance bandwidth becomes narrow. As a result, $W_{p2} = 3.04$ mm is selected for the stable gain and the proposed frequency band.

B. EFFECT OF THE METASURFACE

A metamaterial should possess the unique electromagnetic properties that are caused by the periodic current distribution. Fig. 6 shows the periodic current distribution at the notch frequency band of 6.6 GHz. The three adjacent I-shaped elements generate a pair of ring-road current distributions. At t = 0, the left ring-road current flows in the counterclockwise direction, while the right one flows in the clockwise direction. In addition, the current intensity gets maximum. Then at t = T/4, the current intensity becomes minimum, while the direction of current keeps the same as the one at t = 0. At t = T/2, the direction of current turns to be the opposite to the one at t = T/4, while the current intensity achieves the maximum again. Finally, at t = 3T/4, the direction of current keeps constant and the current intensity becomes minimum again. Here, the periodic current distribution may benefit the antenna gain, however, most of

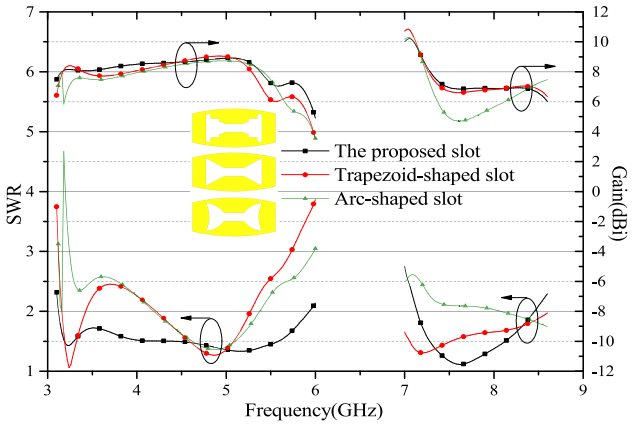

FIGURE 4. SWR and gain with different-shaped slots.

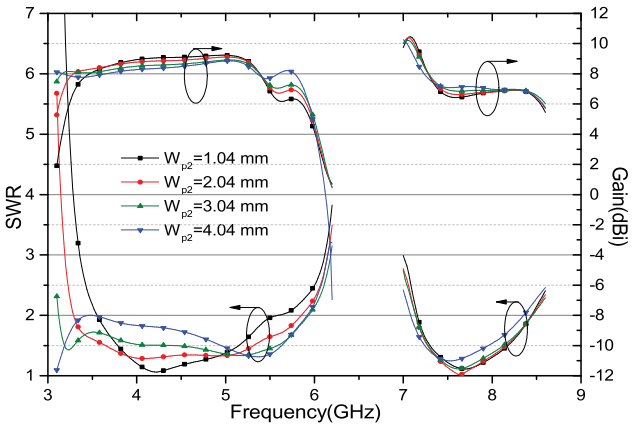

FIGURE 5. SWR and gain with different arc-height W_{p2}.

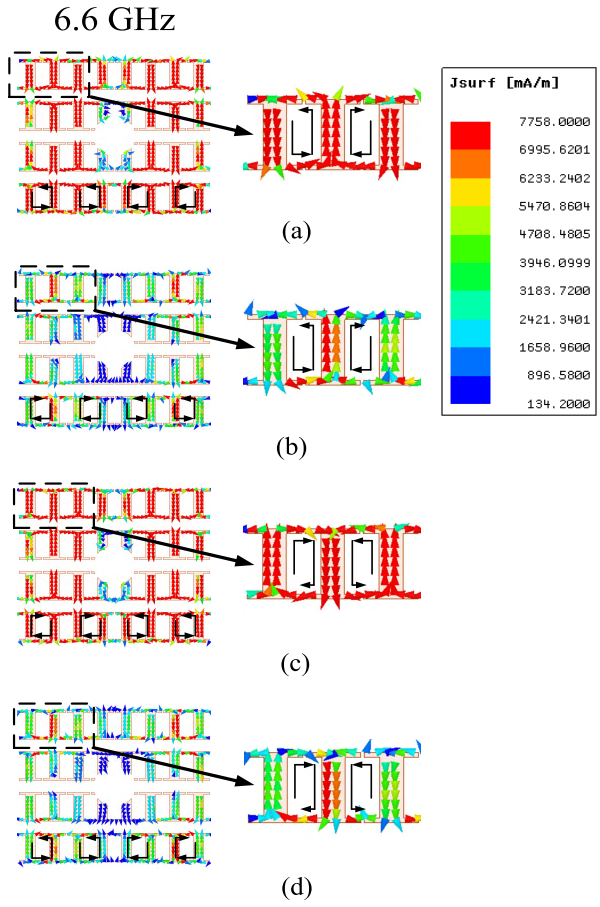

FIGURE 6. Current distributions on the metasurface. (a) t = 0. (b) t = T/4. (c) t = T/2. (d) t = 3T/4.

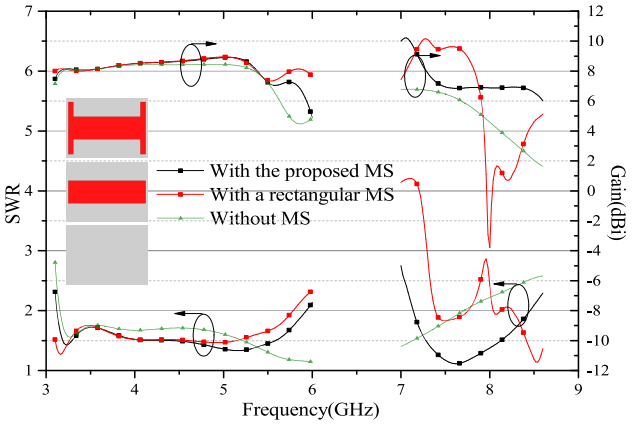

FIGURE 7. SWR and gain with different metasurface structures.

the current on the radiated electric dipole will couple to the MS and hence the notch band will be generated. In other words, the dual wide band instead of a single wide band can be formed.

To reveal the effect of the metasurface, different shapes of metasurface are used to compare in the aspects of SWR, gain and patterns, as shown in Fig. 7. It can be easily seen that without MS the gain is lower than the other two. This is because the MS is equal to an additional quarter-wavelength reflected patch and hence the effective radiated area can be increased. In the lower frequency band, there is no obvious change in the SWR and gain between the rectangular and the proposed MS patches. However, in the upper frequency band, as the frequency increases, by using the rectangular MS there is significant fluctuation in SWR. Therefore, the corresponding gain declines sharply. Here, the proposed MS is not only beneficial to improve gain but also good to broaden the impedance bandwidth. To further study the phenomena, the radiation patterns at 7.8 GHz are shown in Fig. 8. Without the MS or with the rectangular MS patches, the cross-polarization in H-plane is larger than the proposed one. In addition, with the rectangular MS patches, the 3-dB beamwidth in H-plane becomes narrow and the co-polarization radiation in E-plane divides into three parts. Here, the gain in the boresight gets worse. Hence, the proposed MS is superior to the other two.

C. EFFECT OF THE FEEDING STRUCTURE AND THE SHORTED WALL

According to [24], a typical η-shaped feeding strip can be divided into two parts: the transmission line and the coupling strip. Furthermore, the coupling strip is composed of the horizontal and vertical portions. They are critical to the

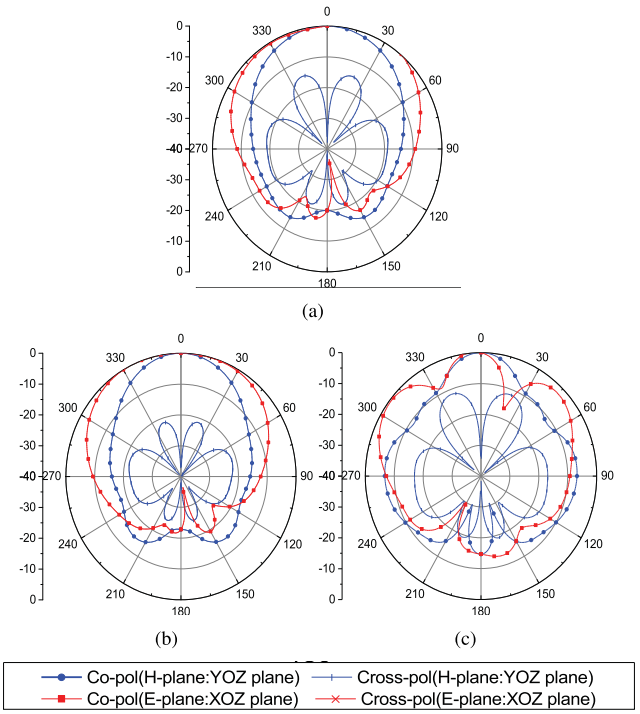

FIGURE 8. Simulated radiation patterns of a single antenna element at 7.8 GHz with different MS structures. (a) Without MS. (b) The proposed MS. (c) With the different MS.

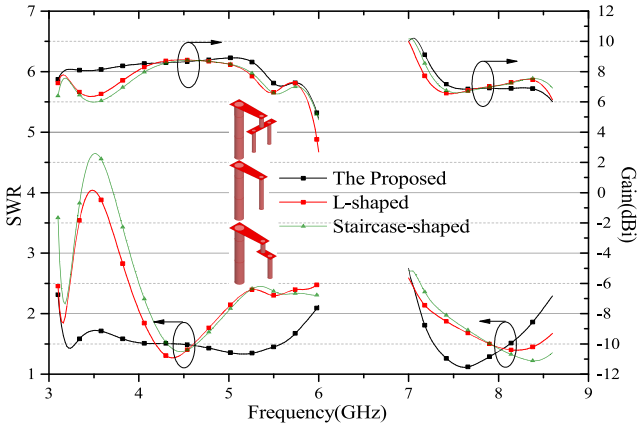

FIGURE 9. SWR and gain with different feeding structures.

impedance bandwidth of the antenna. In our design, in order to obtain flexible impedance matching and much longer effective electric length in such a limited space, the feeding structure is designed as the forked shape as shown in Fig. 9. In the lower frequency band, by using the proposed feeding structure, the most stable and the smallest SWR can be obtained and hence the widest bandwidth can be achieved. Correspondingly, the most stable and the highest gain can be acquired. In the upper frequency band, by adopting the proposed structure, the proposed band can cover the X-band while the other two can not cover it. In addition, the proposed gain is slightly more stable than the other

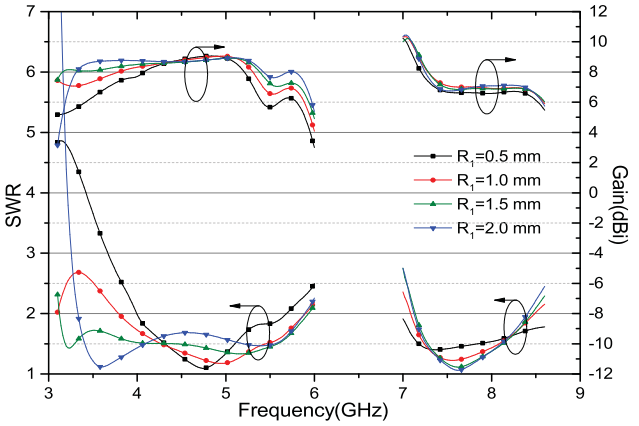

FIGURE 10. Effect of the shorted wall with different R_1.

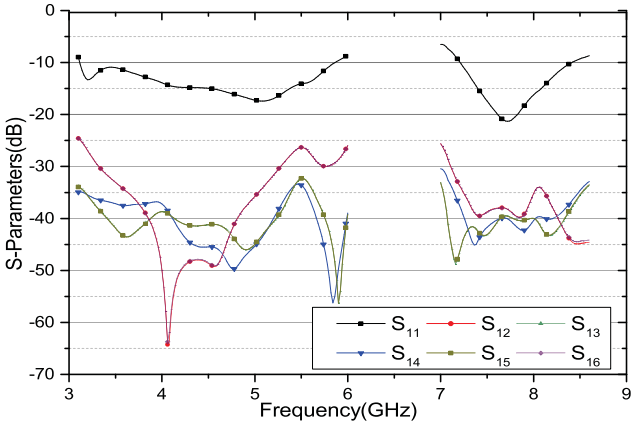

FIGURE 11. S-Parameters of the MIMO System.

two. Noting that the radius of the via shorted wall (R_1) is another key parameter to the SWR and gain. As shown in Fig. 10, in the lower frequency band, the impedance bandwidth becomes wide firstly and then gets narrow as the value of the radius increases. While the corresponding gain becomes more stable. In contrast, there is no obvious change in the upper frequency band. To obtain the most stable gain and the suitable bandwidth, $R_1 = 1.5$ mm is chosen.

D. EFFECT OF THE MIMO SYSTEM

To reduce the size of its MIMO system and improve the coverage in the meantime, a 3D hexagonal structure is introduced because the 3-dB beamwidth of each element is about 60°, as is shown in Fig. 1(d). In addition, in order to reduce the mutual coupling, the six antenna elements are arranged rotationally with an interval of 60°. Fig. 11 shows that the simulated impedance bandwidth (S_{11}) is stable, which ranges from 3.12 GHz to 5.92 GHz, and from 7.14 GHz to 8.45 GHz, respectively. The S-parameters of S_{12}, S_{13} and S_{14} are all below -25 dB. Furthermore, the ECC curves are shown in Fig. 12. In the desired frequency band, all of the ECCs are lower than 350 ppm. In other words, their mutual coupling can be reduced effectively and port isolation can also

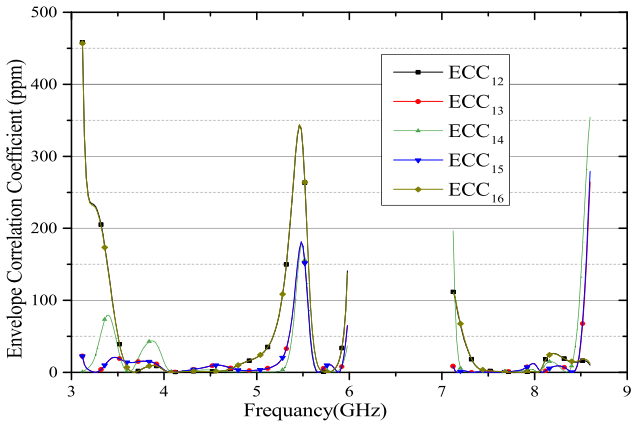

FIGURE 12. Simulated ECC of the MIMO System.

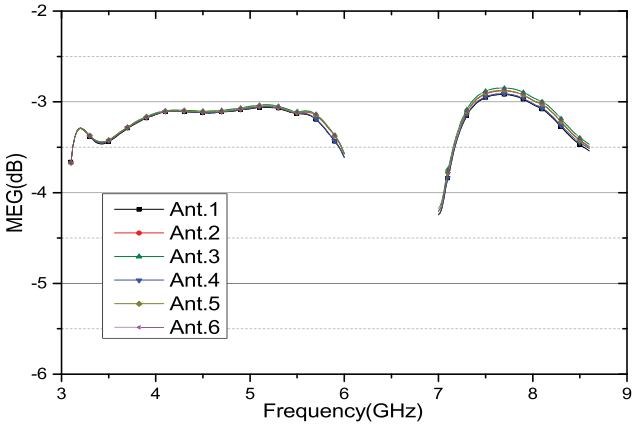

FIGURE 13. Simulated MEG of the MIMO system.

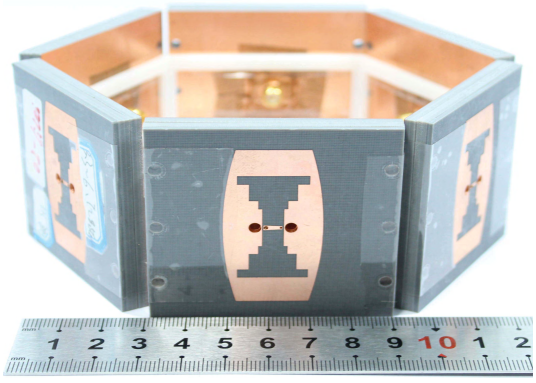

FIGURE 14. Prototypes of the proposed antenna and its MIMO system. 3D view of MIMO antenna system prototype.

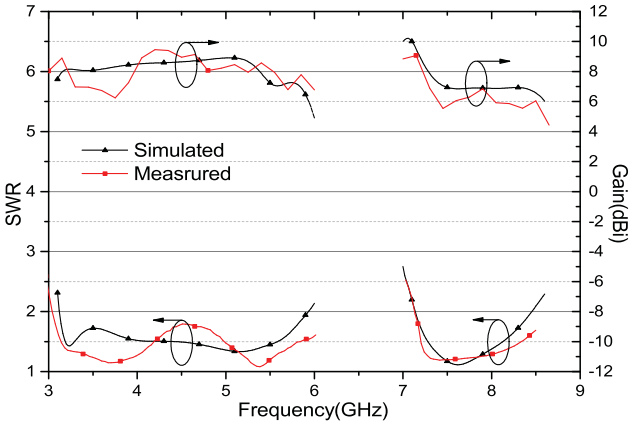

FIGURE 15. Simulated and measured SWR and gains of a single antenna element.

be improved obviously. Besides, owing to the special design, six unidirectional patterns aiming at 0°, 60°, 120°, 180°, 240°, 300° and 360° in the azimuth plane can be obtained across the whole frequency band. Finally, the MEG curves of the MIMO antenna system are shown in Fig. 13. Nearly the same MEG parameters can also be achieved and it means that performance of any antenna element is identical in the MIMO system.

IV. RESULTS AND DISCUSSION

To verify the proposed design, the single antenna element and its MIMO system were fabricated and measured. The results of SWRs, gains, ECC, mean effective gain (MEG), radiation efficiency and radiation patterns were attained, which are the critical parameters of one ME dipole antenna and MIMO system.

As shown in Fig. 15, the simulated impedance bandwidth of the single antenna element ranges from 3.12 to 5.92 GHz, 7.14 to 8.45 GHz ($SWR \leq 2$) for the lower and upper frequency bands, respectively, while the simulated gain varies between 6.0 dBi and 8.9 dBi in the lower band, and between 6.7 dBi and 9.6 dBi in the upper band, respectively. Both of them cover the 5G/WLAN/WiMAX/X-Band frequency bands used in China (eg. 3.3GHz-3.6GHz, 4.8GHz-5GHz, 5.2GHz-5.9GHz, 7.15GHz-8.25GHz). Correspondingly, the measured impedance bandwidth ranges from 3.1 to 6.2 GHz, 7.1 to 8.7 GHz ($SWR \leq 2$) for the lower and upper frequency bands, respectively. And the measured gain varies between 6.1 dBi and 9.1 dBi in the lower band, and between 5.6 dBi and 9.2 dBi in the upper band, respectively. Hence, the gains are relatively stable and high enough for the 5G/WLAN/WiMAX/X-Band communications.

Fig. 16 shows the radiation patterns of the single antenna element at different frequencies. Nearly symmetric unidirectional radiation patterns in the E- and H-planes over the operating frequency range can be obtained. Besides, the cross-polarization levels in E- and H-planes are generally below −22 dB while the front-to-back ratios are larger than 18 dB. However, the co-polarization in H-plane becomes narrow and the cross-polarization in H-plane gets large as the frequency increases due to the higher mode, while there are no obvious changes with the co-polarization and the cross-polarization in E-plane, such as the radiation pattern at 7.8 GHz. In general, the H-plane can nearly provide a stable coverage of about 60° in the operating frequency band except at X-band. Hence the six-element MIMO system can provide

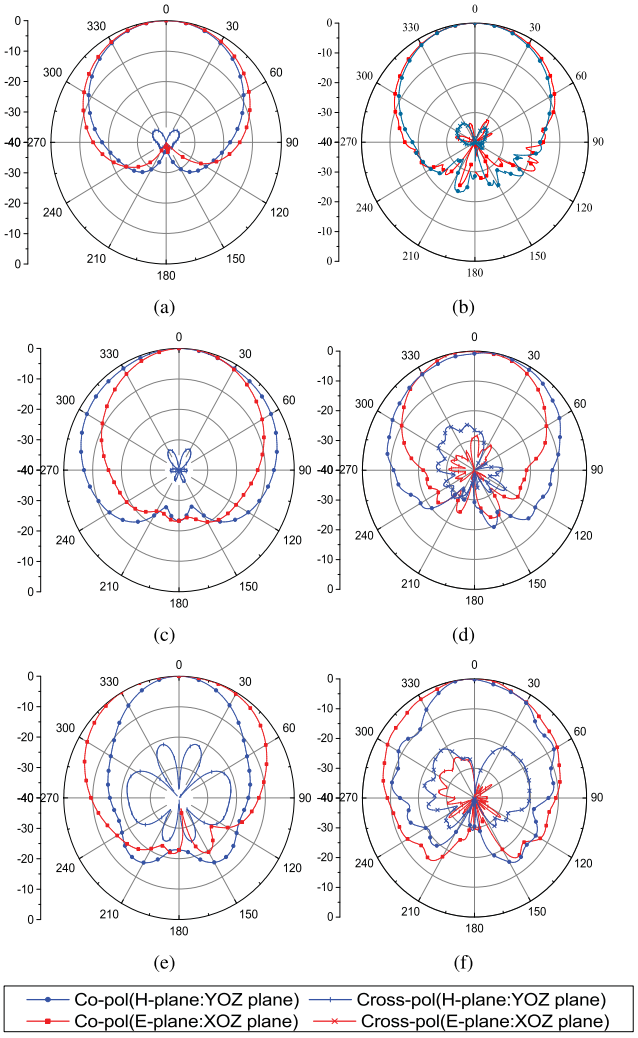

FIGURE 16. Simulated and measured radiation patterns of a single antenna element at 3.4, 5.5 and 7.8 GHz. (a) 3.4 GHz(simulated). (b) 3.4 GHz(measured). (c) 5.5 GHz(simulated). (d) 5.5 GHz(measured). (e) 7.8 GHz(simulated). (f) 7.8 GHz(measured).

a nearly 360° omnidirectional coverage. The measured results are in general agreement with the simulated data except some fabrication errors. Fig. 17 shows the radiation efficiency of an antenna element during the desired frequency band. The radiation efficiency fluctuates around 85% and 80% in lower and upper frequency bands, respectively. Here, with the MS, there is almost no influence on the radiation efficiency and it is high enough for the 5G communication.

In addition, the measured ECC and MEG curves of the MIMO antenna system are shown in Figs. 18 and 19, respectively. The measured values of the ECC are all below 300 ppm due to the comformal design. Generally, the ECC values which are below 0.5 are used to judge whether one MIMO antenna system can provide good pattern diversity. As for the measured MEG curves, they are also nearly the same with each other. It means that the polarized performance of each antenna element is nearly identical. Also, the measured results accord well with the simulation results except some measurement errors.

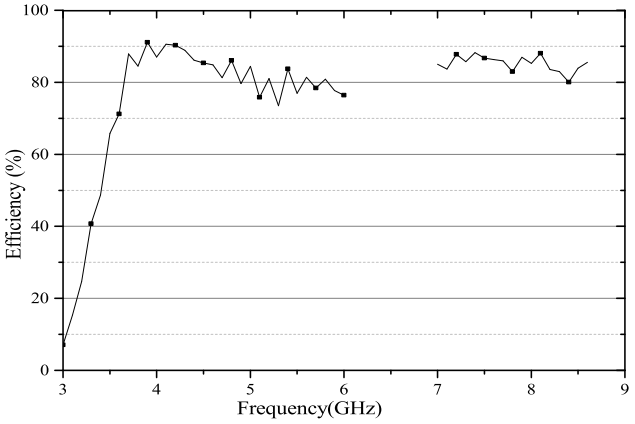

FIGURE 17. Measured radiation efficiency of an antenna element.

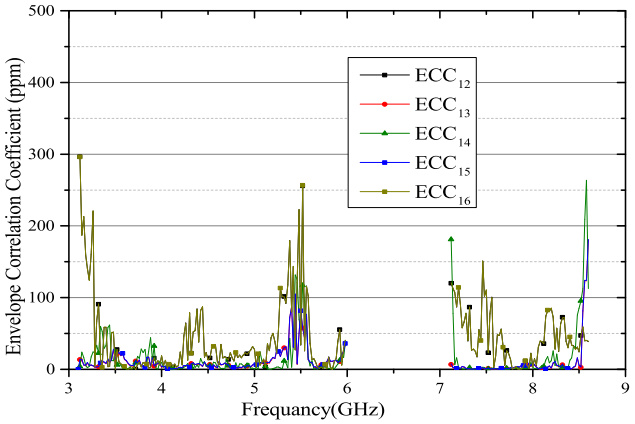

FIGURE 18. Measured ECC of the MIMO System.

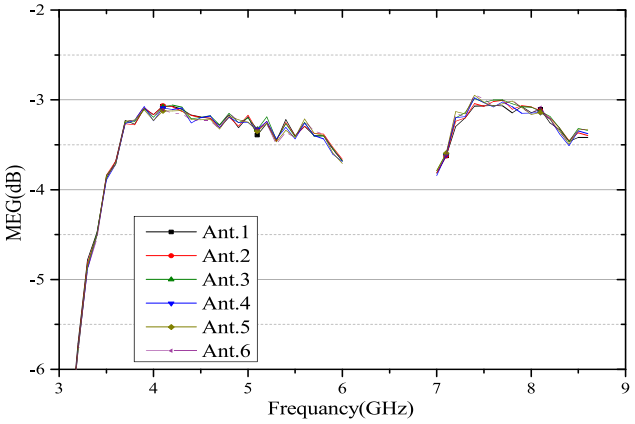

FIGURE 19. Measured MEG of the MIMO ystem.

Table 2 shows comparison between the proposed antenna and other referenced MIMO antennas in terms of bandwidth, average gain, ECC, MEG, the numbers of elements and size. It can be easily observed that the proposed antenna owns the wider bandwidth, the higher and more stable gain, the lower ECC and the smaller size. In addition, the proposed antenna owns the dual-wideband feature. This is because the elements which are printed on the compact planar multi-substrates are arranged on the 3D hexagonal structure.

TABLE 2. Comparison of the proposed antenna with other referenced antennas.

Refs.	Bandwidth (Relative BW/GHz)	Average Gain (dBi)	ECC (<)	The Number Of The Elements	Element Size (λ_0^3)	Remarks
The Proposed Antenna Element	66.7%(3.1∽6.2) 20.3%(7.1∽8.7)	7.6; 7.4.	\	1	0.62×0.62×0.082	Dual-Wideband Bandwidth; High Gain.
The Proposed Antenna MIMO System	55.2%(3.12∽5.88) 15.5%(7.2∽8.41)	\	5×10^{-4}	6	1.27×1.27×0.62	Dual-Wideband Bandwidth; Low ECC; Ideal MEG.
[2]	15.7%(0.82∽0.96) 44.5%(1.71∽2.69) 5.7%(3.4∽3.6)	0±0.5; 2.4±1.3; 2.6±0.6.	0.4	10	0.38×0.19×0.013	Low Gain.
[7]	38.7%(1.77∽2.62)	1.3	1×10^{-3}	4	0.65×0.65×0.70	Low Gain.
[8]	9.8%(2.33∽2.57) 21.7%(4.94∽6.34)	5; 6.	\	12	1.24×1.24×0.47	Narrow Bandwidth; Low Gain.
[13]	34%(0.78∽1.1) 49.5%(1.58∽2.62)	7; 8.	\	1	0.57×0.57×0.15	Dual-Wideband Bandwidth; Bulky Structure.
[14]	8.1%(2.38∽2.58) 60.3%(3.2∽5.96)	4.3; 7.5.	\	1	2.38×2.38×0.65	Narrow Bandwidth In The Upper Band; Bulky Structure.
[16]	18.74%(4.98∽6.01)	6.4	\	1	0.61×0.61×0.07	Low Gain.
[17]	21.5%(2.9∽3.6) 26.5%(4.9∽6.4)	3.3; 3.7.	\	1	0.77×1.06×0.46	Low Gain.
[18]	110%(3.1∽10.7)	8.5	\	1	0.64×0.33×0.08	Unstable Gain.
[19]	17.6%(2.27∽2.7)	\	\	1	0.91×0.91×0.07	Narrow Bandwidth.
[20]	11.43%(3.3∽3.7)	7.5	\	1	0.86×0.86×0.03	Narrow Bandwidth.
[23]	31.8%(1.57∽3.03)	5.9	\	1	1.57×1.57×0.16	Low Gain.

Where λ_0 is the free-space wavelength at the initial frequency.

V. CONCLUSION

A substrate integrated ME dipole antenna with metasurface is proposed for the 5G/WiMAX/WLAN/X-Band MIMO applications. By combining the inherent advantages of ME dipole and metasurface, the low-profile, dual wideband and high-gain features can be achieved. As a result of the 3D hexagonal structure, the good ECC and MEG performance have been obtained. Further more, nearly 360° omnidirectional coverage of H-plane in the operating frequency band has been acquired for the MIMO antenna system. With the above-mentioned characteristics, the proposed antenna is an excellent candidate for the 5G/WiMAX/WLAN/X-Band MIMO communications.

REFERENCES

[1] *Chinese Ministry of Industry and Information Technology Allocates Spectrum for the Fifth Generation Mobile Communication*. Accessed: Nov. 15, 2017. [Online]. Available: http://www.miit.gov.cn/n1146295/n1652858/n1652930/n3757020/c5907905/content.html

[2] Y.-L. Ban, C. Li, C.-Y.-D. Sim, G. Wu, and K.-L. Wong, "4G/5G multiple antennas for future multi-mode smartphone applications," *IEEE Access*, vol. 4, pp. 2981–2988, 2016.

[3] M.-Y. Li *et al.*, "Eight-port orthogonally dual-polarized antenna array for 5G smartphone applications," *IEEE Trans. Antennas Propag.*, vol. 64, no. 9, pp. 3820–3830, Sep. 2016.

[4] K. L. Wong, J. Y. Lu, L. Y. Chen, W. Y. Li, Y. L. Ban, and C. Li, "16-antenna array in the smartphone for the 3.5-GHz MIMO operation," in *Proc. Asia–Pacific Microw. Conf. (APMC)*, vol. 1, Dec. 2015, pp. 1–3.

[5] Y. Li, C.-Y.-D. Sim, Y. Luo, and G. Yang, "12-port 5G massive MIMO antenna array in sub-6 GHz mobile handset for LTE bands 42/43/46 applications," *IEEE Access*, vol. 6, pp. 344–354, 2017.

[6] Q.-L. Yang, Y.-L. Ban, K. Kang, C.-Y.-D. Sim, and G. Wu, "SIW multi-beam array for 5G mobile devices," *IEEE Access*, vol. 4, pp. 2788–2796, 2016.

[7] S. Chen and K.-M. Luk, "A dual-mode wideband MIMO cube antenna with magneto-electric dipoles," *IEEE Trans. Antennas Propag.*, vol. 62, no. 12, pp. 5951–5959, Dec. 2014.

[8] J. J. Liang, J. S. Hong, J. B. Zhao, and W. Wu, "Dual-band dual-polarized compact log-periodic dipole array for MIMO WLAN applications," *IEEE Antennas Wireless Propag. Lett.*, vol. 14, pp. 751–754, 2015.

[9] J. Zhu, S. Liao, S. Li, and Q. Xue, "Wideband low-profile highly isolated MIMO antenna with artificial magnetic conductor," *IEEE Antennas Wireless Propag. Lett.*, vol. 17, no. 3, pp. 458–462, Mar. 2018.

[10] C.-Y.-D. Sim, Y.-K. Shih, and M.-H. Chang, "Compact slot antenna for wireless local area network 2.4/5.2/5.8 GHz applications," *IET Microw., Antennas Propag.*, vol. 9, no. 6, pp. 495–501, Apr. 2015.

[11] B. Yu, K. Yang, C.-Y.-D. Sim, and G. Yang, "A novel 28 GHz beam steering array for 5G mobile device with metallic casing application," *IEEE Trans. Antennas Propag.*, vol. 66, no. 1, pp. 462–466, Jan. 2018.

[12] J. Zhu, S. Li, B. Feng, L. Deng, and S. Yin, "Compact dual-polarized UWB quasi-self-complementary MIMO/diversity antenna with band-rejection capability," *IEEE Antennas Wireless Propag. Lett.*, vol. 15, pp. 905–908, 2016.

[13] W. X. An, H. Wong, K. L. Lau, S. F. Li, and Q. Xue, "Design of broadband dual-band dipole for base station antenna," *IEEE Trans. Antennas Propag.*, vol. 60, no. 3, pp. 1592–1595, Mar. 2012.

[14] B. Feng, J. Zhu, L. Deng, W. An, and Q. Zeng, "A printed dual-wideband magneto-electric dipole antenna and its MIMO system for WLAN and WiMAX applications," in *Proc. IEEE Int. Conf. Comput. Electromagn. (ICCEM)*, Feb. 2016, pp. 256–258.

[15] B. Feng, W. An, S. Yin, L. Deng, and S. Li, "Dual-wideband complementary antenna with a dual-layer cross-ME-dipole structure for 2G/3G/LTE/WLAN applications," *IEEE Antennas Wireless Propag. Lett.*, vol. 14, pp. 626–629, 2015.
[16] H. W. Lai and H. Wong, "Substrate integrated magneto-electric dipole antenna for 5G Wi-Fi," *IEEE Trans. Antennas Propag.*, vol. 63, no. 2, pp. 870–874, Feb. 2015.
[17] B. Feng, Q. Zeng, and M. Wang, "Substrate integrated magneto-electric dipole antenna for WLAN and WiMAX applications," in *Proc. IEEE MTT-S*.
[18] K. Kang, Y. Shi, and C.-H. Liang, "Substrate integrated magneto–electric dipole for UWB application," *IEEE Antennas Wireless Propag. Lett.*, vol. 16, pp. 948–951, Feb. 2017.
[19] H. L. Zhu, S. W. Cheung, K. L. Chung, and T. I. Yuk, "Linear-to-circular polarization conversion using metasurface," *IEEE Trans. Antennas Propag.*, vol. 61, no. 9, pp. 4615–4623, Sep. 2013.
[20] H. L. Zhu, S. W. Cheung, X. H. Liu, and T. I. Yuk, "Design of polarization reconfigurable antenna using metasurface," *IEEE Trans. Antennas Propag.*, vol. 62, no. 6, pp. 2891–2898, Jun. 2014.
[21] H. Zhu, S. W. Cheung, and T. I. Yuk, "Enhancing antenna boresight gain using a small metasurface lens: Reduction in half-power beamwidth," *IEEE Antennas Propag. Mag.*, vol. 58, no. 1, pp. 35–44, Feb. 2016.
[22] L. Mingjian, K.-M. Luk, K. Zhang, and L. Ge, "Miniaturization of magnetoelectric dipole antenna by using metamaterial loading," *IEEE Trans. Antennas Propag.*, vol. 64, no. 11, pp. 4914–4918, Nov. 2016.
[23] M. Martinis, L. Bernard, K. Mahdjoubi, R. Sauleau, and S. Collardey, "Wideband antenna in cavity based on metasurfaces," *IEEE Antennas Wireless Propag. Lett.*, vol. 15, pp. 1053–1056, 2016.
[24] K.-M. Luk and H. Wong, "A new wideband unidirectional antenna element," *Int. J. Microw. Opt. Technol.*, vol. 1, no. 1, pp. 35–44, Jun. 2006.
[25] ANSYS Corporation. *HFSS: High Frequency Structure Simulator Based on the Finite Element Method*. Accessed: Jun. 20, 2018. [Online]. Available: https://www.ansys.com

BOTAO FENG (M'14) received the B.S. and M.S. degrees in communication engineering from the Chongqing University of Posts and Telecommunications, Chongqing, China, in 2004 and 2009, respectively, and the Ph.D. degree in communication and information system from the Beijing University of Posts and Telecommunications, Beijing, China, in 2015. He joined the Dongguan Branch of Nokia Mobile Phones Ltd., China, as a Senior Communication Engineer, in 2004. From 2009 to 2012, he served as a Senior Research Fellow in charge of mobile network optimization with China United Network Communications Company Ltd. He is currently a Postgraduate Advisor and a Post-Doctoral Advisor with Shenzhen University, Shenzhen, Guangdong, China. He is also the Head of the Laboratory of Wireless Communication, Antennas and Propagation, Shenzhen University, the Director of the Joint Laboratory of Antenna and Electromagnetic Propagation, Shenzhen University-Rihai Communication Technology Company Ltd., and the Director of the Joint Laboratory of Antenna and Microwave Technology, Shenzhen University-Skywave Communication Technology Company Ltd. He and his team members are currently conducting over 10 projects on antenna development and design for 5G and future communications, which are supported by natural science research funds and industrial cooperation research and development funds. He has authored over 30 SCI- and EI-indexed papers, and holds 10 invention patents. His research interests include base station antenna, microcell antenna, indoor antenna, and wireless network optimization. He serves as a peer reviewer for several IEEE/IET journals and a technical committee member for conferences on microwave technique and antenna.

JIEXIN LAI was born in Zhanjiang, Guangdong, China, in 1993. He received the B.S. degree from Shenzhen University in 2016, where he is currently pursuing the M.S. degree. His research interests include wideband antenna, indoor antenna, miniaturized antenna, and so on.

QINGSHENG ZENG (S'97–M'02–SM'11) received the Ph.D. degree from the University of Ottawa, Canada. He has been a Research Engineer and a Senior Research Engineer with the Communications Research Centre Canada, Canada. He is currently a Distinguished Professor and a Ph.D. Advisor with the Nanjing University of Aeronautics and Astronautics, an Adjunct Professor and a Ph.D. Advisor with the University of Ottawa, Carleton University, Université du Québec an Outaouais, the Institut National de la Recherche Scientifique—Centre Energie, and Matériaux et Télécommunications (INRS-EMT), and a Guest Professor with Harbin Engineering University, Northwestern Polytechnic University, the Beijing University of Post and Telecommunications, and Beijing Jiaotong University. He has undertaken research and teaching in several fields, including antenna analysis and design, electromagnetic compatibility and interference (EMC/EMI), ultra wideband technology, radio wave propagation, and computational electromagnetics. He is a member of the IEEE Canada Industry Relations Committee. He has been a member of the Strategic Projects Grant Selection Panel (Information and Communications Technologies B) for the Natural Sciences and Engineering Research Council of Canada (NSERC), a member of the Site Visit Committee of the NSERC Industrial Research Chair, and a Reviewer of NSERC Industrial Research and Development Fellowships. He is the Chair of the Antennas and Propagation/Microwave Theory and Techniques Joint Chapter and the Secretary of the EMC Chapter of the IEEE Ottawa.

His work on the project Aggregate Interference Analysis and Suitability of Some Propagation Models to Ultra-wideband Emissions in Outdoor Environments has formed one part of the Consultation Paper on the Introduction of Wireless Systems Using Ultra Wideband Technology, Spectrum Management and Telecommunications Policy, Industry Canada, and has been taken as a significant contribution to the International Telecommunication Union. He has published over 100 SCI and EI indexed papers and technical reports, authored one book and co-authored two book chapters, one of which has been downloaded over 3000 times only in one year after it was published in 2011. He received several technical and technical service awards, was ranked as one of the researchers at the Communications Research Centre Canada with the strongest impacts in 2011, and selected as a Distinguished Expert under the Plan of Hundreds of Talents of Shanxi Province in China in 2015 and an Oversea Prestigious Advisor of Guangdong Province in 2017. He has been serving as an editorial board member and a reviewer for a number of technical books and scientific journals, and a conference co-chair, a session chair, an organizer, a technical program committee co-chair, a member, a reviewer, a short course/workshop/tutorial presenter, and a keynote speaker for many international and national symposia.

KWOK L. CHUNG (S'00–M'05–SM'11) received the B.E. (Hons.) and Ph.D. degrees in electrical engineering from the University of Technology Sydney, Australia, in 1999 and 2005, respectively. He joined the Faculty of Engineering, University of Technology Sydney, in 2004, as a Lecturer. In 2006, he joined The Hong Kong Polytechnic University, where he spent about six years in the teaching of electronic engineering. In 2012, he joined the Institute for Infrastructure Engineering, University of Western Sydney, as a Research Fellow. In 2015, he joined the Qingdao University of Technology (QUT), China, as a Cross-Disciplinary Research Professor and a Supervisor of Ph.D. students. He has authored and coauthored about 100 publications (SCI and EI) in various areas of electrical and civil engineering. His current research interests include passive wireless sensors for structural health monitoring, cement-based materials design and characterization, microwave antennas, metasurface designs, and so on. He is a Core Member of the Taishan Scholar Priority Discipline Talent Group, QUT, where he is also a member of International Steering Committee of the IEEE International Workshop on Electromagnetics. He was the Vice Chair and the Chairman of the IEEE AP/MTT Hong Kong joint chapter in 2010 and 2011, respectively. He acts as a Reviewer of numerous IEEE, IET, Elsevier, and other international journals. He has been the Founding Chair of the IEEE Qingdao AP/MTT/COM joint chapter since 2017. He is currently an Associate Editor of the IEEE Access.